ACS Catalysis

pubs.acs.org/acscatalysis

Research Article

Unraveling the Hydrolysis of Z_2Cu^{2+} to $ZCu^{2+}(OH)^-$ and Its Consequences for the Low-Temperature Selective Catalytic Reduction of NO on Cu-CHA Catalysts

Wenshuo Hu, Umberto Iacobone, Federica Gramigni, Yu Zhang, Xiaoxiang Wang, Shaojun Liu, Chenghang Zheng, Isabella Nova, Xiang Gao,* and Enrico Tronconi*

Cite This: *ACS Catal.* 2021, 11, 11616–11625

Read Online

ABSTRACT: As the state-of-the-art catalyst for the selective catalytic reduction (SCR) of NO*x*, Cu-CHA has been extensively investigated in both its practical and fundamental aspects. Among the latter, how Z_2Cu^{2+}, an active site for SCR, participates in low-temperature (LT) SCR reactions remains debated. Here, we propose a scheme involving the hydrolysis of Z_2Cu^{2+} to $ZCu^{2+}(OH)^-$, a thermodynamically and kinetically favorable process under LT-SCR conditions, based on multiple pieces of evidence from a probe reaction (transient CO oxidation), transient Cu^{2+} reduction kinetic runs, in situ FTIR spectroscopy, and first-principles calculations. Such an integrated investigation reveals unambiguously that the hydrolysis of Z_2Cu^{2+} to $ZCu^{2+}(OH)^-$ occurs facilely in the presence of NH_3, which may thus reconcile the identical quadratic kinetics of $Z_2Cu^{2+}/ZCu^{2+}(OH)^-$ reduction with the inactivity of Z_2Cu^{2+} in the formation of Cu^{2+} pairs. Accordingly, we highlight that NH_3-assisted hydrolysis plays a critical role in LT-SCR and should be taken into account especially when discussing SCR reaction details over Z_2Cu^{2+}.

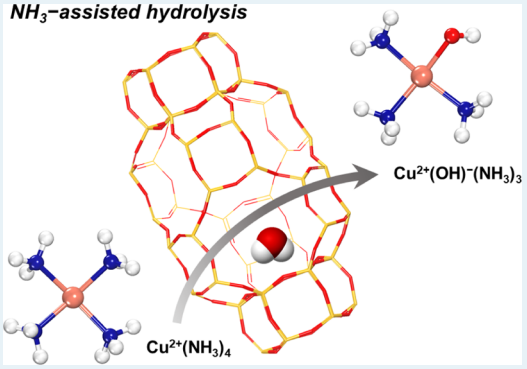

KEYWORDS: *low-temperature SCR, Cu-CHA, hydrolysis, Cu speciation, Z_2Cu^{2+}, $ZCu^{2+}(OH)^-$*

1. INTRODUCTION

Copper-exchanged small-pore zeolites, Cu-CHA, are nowadays the state-of-the-art catalysts for the NO*x* abatement via selective catalytic reduction (SCR) in diesel emission control.[1−3] Research on fundamental aspects such as characterization of active sites in response to real, dynamic SCR working conditions[4−7] and elementary/pseudoelementary steps addressing reaction mechanisms[8−11] has been extensively conducted to reveal the catalytic chemistry underlying the conspicuous performance of Cu-CHA in terms of both low-temperature (LT) SCR activity and hydrothermal durability. As now widely accepted in the field,[2,4−6,12] two types of Cu^{2+} cations, namely, Z_2Cu^{2+} with each Cu^{2+} balancing two proximate Al within the zeolite framework (denoted as Z_2) and $ZCu^{2+}(OH)^-$ with Cu^{2+} balancing one Al (Z) together with a hydroxyl group, are regarded as precursors for the active sites catalyzing SCR reactions. In particular, these two Cu^{2+} cations are found fully coordinated with NH_3 molecules and detached from the CHA framework under LT-SCR conditions, being $Cu^{2+}(NH_3)_4$ and $Cu^{2+}(OH)^-(NH_3)_3$, respectively.[5,12,13] According to previous work, two model Cu-CHA samples dominated by Z_2Cu^{2+} and $ZCu^{2+}(OH)^-$, respectively, showed comparable kinetics during steady-state LT-SCR,[5] which suggests an equivalent activity of these two Cu^{2+} species despite their structural difference. Consistently, density functional theory (DFT) calculations[5] revealed that NO-assisted NH_3 activation is able to reduce Cu^{2+} to Cu^+ (reduction half-cycle of LT-SCR, RHC) and has similar activation barriers on monomeric $Cu^{2+}(NH_3)_4$ (+74 kJ mol^{-1}) and $Cu^{2+}(OH)^-(NH_3)_3$ (+71 kJ mol^{-1}); this result, along with the fact that both Cu^{2+} cations are reduced to $Cu^+(NH_3)_2$ and thus identical oxidation half-cycle processes (Cu^+ to Cu^{2+}, OHC) are expected, seems to well explain the observed equivalence of Z_2Cu^{2+} and $ZCu^{2+}(OH)^-$ in steady-state SCR. Recently, however, we found that[14−16] LT-RHC rates show a second-order dependence on Cu^{2+} across a broad array of Cu-CHA catalysts and reaction conditions, which strongly questions RHC mechanisms based on isolated Cu^{2+} cations and, instead, suggests a Cu^{2+} pair mediated LT-RHC pathway. Indeed, NH_3-solvated $ZCu^{2+}(OH)^-$ is able to diffuse through CHA cages and constitutes a dinuclear Cu^{2+} configuration of

Received: June 20, 2021
Revised: August 20, 2021
Published: September 3, 2021

https://doi.org/10.1021/acscatal.1c02761
ACS Catal. 2021, 11, 11616–11625

two proximate $Cu^{2+}(OH)^{-}(NH_3)_3$ units accordingly (called two-P).[14] $Cu^{2+}(NH_3)_4$, however, is only intracage mobile because of strong electrostatic tethering from the CHA framework[5,17] and thus seems unable to directly form the Cu^{2+} pairs needed for LT-RHC reactions. In this context, how $Cu^{2+}(NH_3)_4$ participates in LT-RHC and complies with the quadratic kinetics in Cu^{2+} observed experimentally is still unclear and needs further elucidation.

In this work, we provide a plausible scheme involving the conversion of Z_2Cu^{2+} into $ZCu^{2+}(OH)^{-}$ through hydrolysis reactions, which can effectively reconcile the identical kinetics of these two sites in RHC (both second-order) and the inactivity of Z_2Cu^{2+} in directly forming Cu^{2+} pairs. In doing so, we used transient CO oxidation to CO_2 to directly probe the quantity of intercage mobile Cu^{2+} precursors, that is, $ZCu^{2+}(OH)^{-}$. In fact, this probe reaction is a two-electron event and thus proceeds solely on dinuclear Cu^{2+}.[18−20] Combining this method with transient RHC kinetic experiments, in situ FTIR spectroscopy, first-principles calculations of DFT and ab initio molecular dynamics (AIMD) allow the in situ assessment of reactivity and population of these two Cu^{2+} species and, more importantly, convey a conclusive and novel demonstration of Z_2Cu^{2+} hydrolysis to $ZCu^{2+}(OH)^{-}$ in the presence of NH_3.

2. METHODS

2.1. Experimental Details. *2.1.1. Transient CO Oxidation Tests.* Transient CO oxidation tests were performed over a powdered research Cu-CHA catalyst (Cu = 1.7 wt %, Si/Al = 12.5) provided by Johnson Matthey. Prior to CO oxidation, 32 mg of Cu-CHA catalyst (total Cu loading ≈ 8.9 μmol) with cordierite as the diluent loaded in a quartz microflow reactor (ID ≈ 6 mm) were preconditioned at 873 K for 5 h in 10% H_2O + 10% O_2 (He as the carrier gas). We identify this set of samples as conditioned Cu-CHA hereafter. According to ref 12, NO_2 adsorption + temperature programed desorption (TPD) can be used as an effective approach to quantify populations of $ZCu^{2+}(OH)^{-}$ and Z_2Cu^{2+}, based on which we estimated ∼64% $ZCu^{2+}(OH)^{-}$ in the conditioned Cu-CHA. After conditioning, the catalysts were treated in 8% O_2 at 823 K for 1 h and then cooled down to 473 K. Depending on wet or dry tests, 5% H_2O was selectively added to the gas flow (H_2O remained for the full duration of the wet test), followed by exposing catalysts to 500 ppm NH_3 until saturation, NH_3 cutoff, and isothermal He purge. Note that 8% O_2 was kept in the feed to prevent possible reduction by NH_3. Subsequently, 1000 ppm CO was fed (O_2 off) for 1.5 h, and temporal CO_2 formation was recorded for transient analysis. Finally, the Cu-CHA catalysts were exposed to 500 ppm NO and NH_3 to titrate residual Cu^{2+} after CO oxidation. A total flow rate of 266,250 $cm^3\ h^{-1}\ g_{cat}^{-1}$ (STP) was used, and gaseous species at the reactor outlet were measured by using a mass spectrometer (QGA Hiden Analytical) and a UV analyzer (ABB LIMAS 11 HW) arranged in a parallel configuration. Additional details regarding the rig can be found elsewhere.[14−16,18]

2.1.2. Transient RHC Kinetic Runs. Transient RHC kinetic runs were performed over conditioned and aged Cu-CHA catalysts in the form of powders. The conditioned sample was the same used in the above CO oxidation experiments, while the aged Cu-CHA (Cu = 1.7 wt %, Si/Al = 12.5) was hydrothermally treated at 973 K for 18 h in 10% H_2O + 10% O_2 and was estimated to have ∼20% $ZCu^{2+}(OH)^{-}$ based on NO_2 adsorption + TPD analysis. Previous works[21,22] show that hydrothermal treatments at this level as well as at that used for in situ FTIR experiments (Section 2.1.3) can effectively change $Z_2Cu^{2+}/ZCu^{2+}(OH)^{-}$ proportions while causing no significant damage to Cu-CHA structures. In all microreactor runs, He was used as the carrier gas to enable N_2 detection and closure of the N-balance. A mass spectrometer (QGA Hiden Analytical) and a FTIR gas analyzer (Bruker MATRIX MG2C) arranged in a parallel configuration allowed the simultaneous measurement of all reacting and product species involved (NO, NH_3, NO_2, N_2, N_2O, and H_2O). In general, two types of transient RHC kinetic experiments were conducted starting from (1) oxidative pretreatments or (2) steady-state SCR conditions, respectively.

In test (1), the conditioned and aged Cu-CHA samples were pretreated in 8% O_2 at 823 K for 1 h and then cooled down to the temperatures of interest, after which 500 ppm NH_3 was added to the feed stream until saturation, followed by isothermal purge (NH_3 off) and introduction of 500 ppm NO and NH_3 (O_2 off). Note that this protocol is the same as protocol (ii) used in our previous work.[15]

In test (2), the aged Cu-CHA samples were exposed to standard SCR feed compositions, that is, 500 ppm NO and NH_3 and 8% O_2, until reaching steady state. Then, O_2 was switched off for a transient RHC measurement.

In both tests, 32 mg of Cu-CHA catalysts with cordierite as the diluent and a total flow rate of 450,000 $cm^3\ h^{-1}\ g_{cat}^{-1}$ (STP) were used to enable a direct comparison with the previous work.[15]

2.1.3. In Situ FTIR Spectroscopy. In situ diffuse reflectance infrared Fourier transform spectroscopy experiments were performed on a Nicolet 6700 spectrometer with a mercury cadmium telluride detector cooled by liquid N_2, as detailed elsewhere.[23,24] Spectra in the absorbance mode were recorded at 473 K after hydrothermally aging Cu-CHA (Cu = 2 wt %, Si/Al = 13.5) in the fixed-bed reactor at 923 K for 50 h in 10% H_2O + 10% O_2 [estimated as 15−20% of $ZCu^{2+}(OH)^{-}$] and a subsequent in-cell pretreatment in 10% O_2 at 723 K for 1 h. Background spectra were recorded in flowing 10% O_2 at 473 K after the aforementioned in-cell pretreatment and were subtracted from the sample spectra in order to resolve the changes induced by NH_3, H_2O, and H_2O + NH_3 (see the detailed Results and Discussion below). Accumulation of 8 or 32 scans was obtained at a resolution of 4 cm^{-1}. 500 ppm NH_3, 10% O_2, 2% H_2O (fed by a saturator), and balance N_2 were used in a total flow rate of ∼200,000 $cm^3\ h^{-1}\ g_{cat}^{-1}$ (STP, catalyst load ∼30 mg).

2.2. Computational Details. Rhombohedral CHA unit cells with 12 tetrahedral sites were used[14,16] to construct all structures considered in this work. Two Al atoms were included inside each unit cell to compensate the +2 charge of Cu cations (labeled as Z_2Cu^{2+}). Due to the well-known mobile nature of solvated Cu species in zeolite cages,[5,25,26] we used Born−Oppenheimer AIMD on all structures to seek low-energy configurations from multiple local minima.[5,8,27] Spin-polarized calculations using the Perdew−Burke−Ernzerhof (PBE)[28] generalized gradient approximation (GGA) exchange−correlation functional and the D3 scheme with Becke−Johnson damping[29,30] accounting for long-range van der Waals dispersion interactions were run at 473 K in the canonical ensemble (*NVT*) by a Nosé−Hoover thermostat[31,32] with the Vienna *Ab initio* Simulation Package (VASP).[33] A plane-wave cutoff of 400 eV, a 0.6 fs time step for a total sampling time of 15 ps, and sampling of the first Brillouin zone

https://doi.org/10.1021/acscatal.1c02761
ACS Catal. 2021, 11, 11616−11625

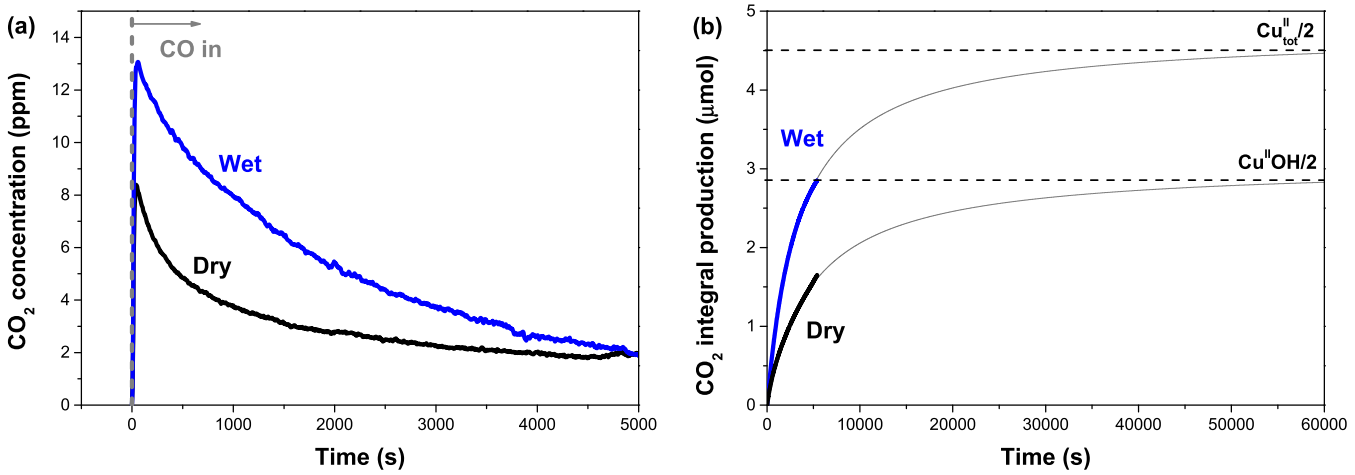

Figure 1. Transient CO oxidation tests over conditioned Cu-CHA (Cu = 1.7 wt %, Si/Al = 12.5) with preadsorbed NH_3 (not shown): dry (black) vs wet (blue). Thin lines in panel b: model predictions from eq 2; thick lines: experimental CO_2 integral production. Reaction conditions: T = 473 K, CO = 1000 ppm, O_2 = 0%, H_2O = 5% (for the wet test), and total flow rate = 266,250 $cm^3\ h^{-1}\ g_{cat}^{-1}$ (STP).

at a single Γ-point were used in all the AIMD calculations. As suggested in a recent work by Chen et al.,[27] the hydrogen mass was replaced by that of tritium to facilitate the integration of motion equations.

Low-energy configurations from AIMD simulations were further optimized by periodic DFT calculations using the projector augmented-wave[34,35] method with the same PBE + D3 approach (VASP[33]). Spin-polarized calculations with 400 eV cutoff and single Γ-point sampling of the k-point were executed with an electronic energy and atomic force convergence criteria of 10^{-6} eV and 0.03 eV $Å^{-1}$,[5,14,16] respectively. Harmonic vibrational frequencies were calculated with a differential displacement of 0.01 Å and were used to compute zero-point vibrational energies. Activation energy (E_a) was calculated by the climbing image nudged elastic band (CI-NEB)[36] method, with identical convergence criteria as in above structure optimizations. Transition states were further confirmed by their one imaginary frequency along the reaction coordinate. We also used the hybrid functional Heyd−Scuseria−Ernzerhof (HSE06)[37−39] with the D3 Becke−Johnson damping scheme to optimize some structures of interest. Results show that energies from GGA and hybrid functionals are very similar in our present case (see S1 in the Supporting Information), thus rationalizing the use of the more cost-effective PBE functional in this work.

We further corrected DFT-computed energies to Gibbs free energy at temperatures of interest and standard pressure (0.1 MPa). Since confined species within zeolite voids are mobile, these retained translations and rotations would lead to the wrong estimation of free energies if ignored. As such, low-frequency vibrational modes were replaced by 2/3 of their "free" translational and rotational entropies and enthalpies.[14,27,40] Based on these free energies, thermodynamic diagrams can be constructed through the van't Hoff equation.

3. RESULTS AND DISCUSSION

3.1. Transient CO Oxidation. As briefly discussed in the Introduction section, CO oxidation to CO_2 involves a two-electron transfer and thus can solely be mediated by dinuclear Cu^{2+} species,[20] as the reduction of each Cu^{2+} to Cu^+ provides one-electron transfer only

$$CO + [Cu{-}O{-}Cu]^{2+} \rightarrow CO_2 + 2Cu^+ \quad \text{(R.1)}$$

This enables the use of transient CO oxidation as a probe reaction to quantify the fraction of dinuclear Cu^{2+}. As revealed by some of us in a dedicated work,[18] the presence of NH_3 significantly increased dry CO oxidation (reflected by Cu^{2+} reduction) from a negligible level (<5% Cu^{2+} reduction) to an obvious extent of 38% Cu^{2+} reduction on a similar compositional Cu-CHA sample. These observations highlight that transient Cu^{2+} pairs, which are formed in situ by NH_3 solvation and mobilization, play a dominant role in this process. Following this thought, we performed dry and wet transient CO oxidation tests after NH_3 preadsorption, as illustrated in Figure 1.

Clearly, CO_2 formation was observed once CO was fed to the reactor (Figure 1a). According to ref 18, the transient CO_2 dynamics can be accurately described by a quadratic rate expression

$$r_{CO_2} = k_{app}\cdot[Cu^{2+}]^2 = -\frac{1}{2}\cdot\frac{d[Cu^{2+}]}{dt} \quad (1)$$

where r_{CO_2} is the rate of CO_2 formation, k_{app} is the apparent rate constant, and $[Cu^{2+}]$ is the concentration of available NH_3-solvated Cu^{2+}. Differential reactor conditions are assumed in view of the limited CO conversions. Integrating eq 1 in time with a proper initial condition of $[Cu^{2+}] = [Cu^{2+}]_0$ (i.e., the amount of Cu^{2+} available before CO oxidation) at t = 0, and considering that the integral production of CO_2 is equal to half the extent of Cu^{2+} reduction (see R.1), gives

$$CO_2\ \text{integral} = \frac{[Cu^{2+}]_0}{2}\cdot\frac{2\cdot k_{app}\cdot[Cu^{2+}]_0\cdot t}{1 + 2\cdot k_{app}\cdot[Cu^{2+}]_0\cdot t} \quad (2)$$

Indeed, eq 2 (thin gray lines in Figure 1b) nicely fits the experimental CO_2 production (thick lines), confirming that this simple kinetic model is able to capture the transient dynamics of the CO oxidation experiments. Furthermore, the asymptotic limit predicted by eq 2 (i.e., $[Cu^{2+}]_0/2$ as $t \rightarrow \infty$) under dry conditions is ~2.83 μmol, exactly half the amount of $ZCu^{2+}(OH)^-$ in the conditioned Cu-CHA catalyst (~2.85 μmol), indicating that only $ZCu^{2+}(OH)^-$, rather than Z_2Cu^{2+}, is relevant in the dry CO oxidation chemistry over Cu-CHA.

https://doi.org/10.1021/acscatal.1c02761
ACS Catal. 2021, 11, 11616−11625

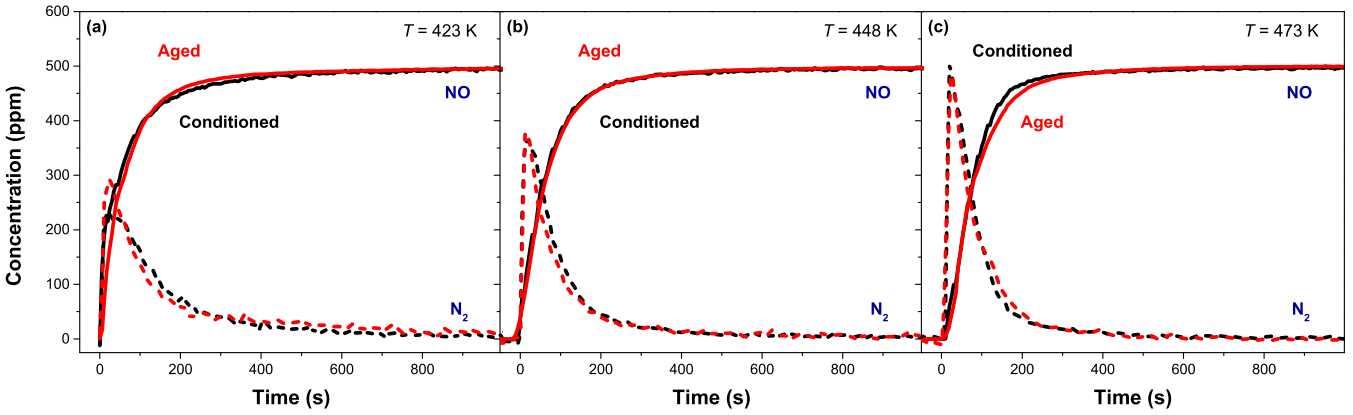

Figure 2. Transient RHC kinetic tests starting from oxidative pretreatments over conditioned (black) and aged (red) Cu-CHA (Cu = 1.7 wt %, Si/Al = 12.5) at (a) 423, (b) 448, and (c) 473 K. NO (solid) and N_2 (dashed) signals are reported. Reaction conditions: NO = NH_3 = 500 ppm, O_2 = H_2O = 0%, and total flow rate = 450,000 $cm^3\ h^{-1}\ g_{cat}^{-1}$ (STP). Data for the conditioned Cu-CHA catalyst are from ref 15.

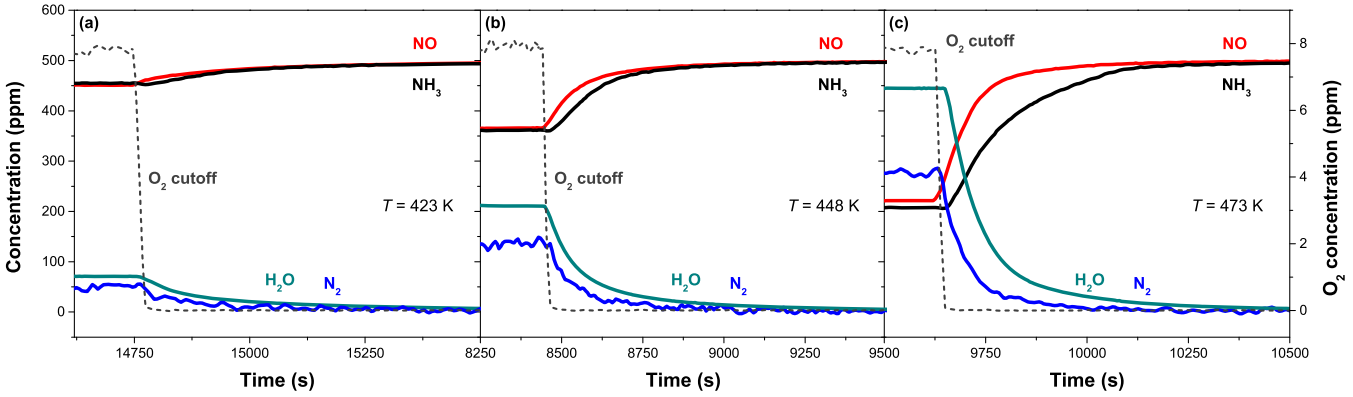

Figure 3. Transient RHC kinetic tests starting from steady-state SCR over aged Cu-CHA (Cu = 1.7 wt %, Si/Al = 12.5) at (a) 423 K, (b) 448 K, and (c) 473 K. Reaction conditions: NO = NH_3 = 500 ppm, O_2 = 8% (when used), H_2O = 0%, and total flow rate = 450,000 $cm^3\ h^{-1}\ g_{cat}^{-1}$ (STP).

This conclusion is fully consistent with both previous CO titration results from some of us[18] and recent in situ UV−vis results[19] reporting that Z_2Cu^{2+}-dominated Cu-CHA samples showed no changes after CO exposure, whereas $ZCu^{2+}(OH)^-$-dominated samples showed substantial Cu^{2+} reduction. Indeed, theory predicts that NH_3-solvated Z_2Cu^{2+} cannot diffuse through CHA cages because of strong electrostatic tethering from the CHA framework;[5,17] thus, direct formation of dinuclear Cu^{2+} from discrete Z_2Cu^{2+} monomers should be negligible. NH_3-solvated $ZCu^{2+}(OH)^-$, in contrast, is a one-charge complex and is therefore intercage mobile and able to cohabit with a second $Cu^{2+}(OH)^-(NH_3)_3$ unit to form Cu^{2+} pairs.[14] Taken all together, these results indicate that CO oxidation actually titrates the population of intercage mobile precursors $ZCu^{2+}(OH)^-$, which are responsible for the transient CO oxidation process.

Interestingly, adding H_2O to the gas flow increased CO_2 formation significantly, as illustrated in Figure 1a. The perfect fit of eq 2 to the "wet" experimental data again confirms the second-order kinetics and thus a Cu^{2+} pair mediated process (Figure 1b). The asymptotic limit of eq 2, ∼4.47 μmol, is now equal to half of the total Cu^{2+} loading (∼4.45 μmol), that is, the sum of Z_2Cu^{2+} and $ZCu^{2+}(OH)^-$, suggesting that all Cu^{2+} cations can form Cu^{2+} pairs and participate in CO oxidation under wet conditions. This result therefore indicates that H_2O mobilizes the relatively "stationary" NH_3-solvated Z_2Cu^{2+} complexes and makes them intercage mobile too. A straightforward scheme accounting for this observation could be related to an increased mobility of Z_2Cu^{2+} due to H_2O coordination. This hypothesis, however, is not compatible with the fact that NH_3 has a much stronger affinity to Cu cations than H_2O;[4,5] thus, the nature of Cu^{2+}−NH_3 complexes should not be significantly affected by the presence of H_2O. An alternative explanation is based on the H_2O-assisted conversion of Z_2Cu^{2+} into $ZCu^{2+}(OH)^-$, enabling Z_2Cu^{2+} to act eventually as intercage mobile NH_3-solvated $ZCu^{2+}(OH)^-$. Next, we try to further probe the plausibility of this proposal.

3.2. Transient RHC Kinetic Analysis. Figure 2 reports transient RHC kinetic experiments over conditioned and aged Cu-CHA. Since the catalysts were preoxidized at 823 K, addition of NO + NH_3 actually reflects the Cu^{2+} reduction process (R.2 and 3, i.e., RHC)[12,14−16]

$$Cu^{2+}(OH)^-(NH_3)_3 + NO \rightarrow Cu^{+}(NH_3)_2 + N_2 + 2H_2O \quad \text{(R.2)}$$

$$Cu^{2+}(NH_3)_4 + NO \rightarrow Cu^{+}(NH_3)_2 + NH_4^{+} + N_2 + H_2O \quad \text{(R.3)}$$

Noticeably, Cu^{2+} reduction dynamics are insensitive to the hydrothermal treatments carried out on the catalysts, as shown in Figure 2 by the overlapping curves of NO and N_2 on conditioned and aged Cu-CHA at three tested temperatures. As mentioned in Section 2.1, the fraction of $ZCu^{2+}(OH)^-$ is ∼64% for the conditioned sample while only ∼20% for the aged one, suggesting that $ZCu^{2+}(OH)^-$ and Z_2Cu^{2+} have

https://doi.org/10.1021/acscatal.1c02761
ACS Catal. 2021, 11, 11616−11625

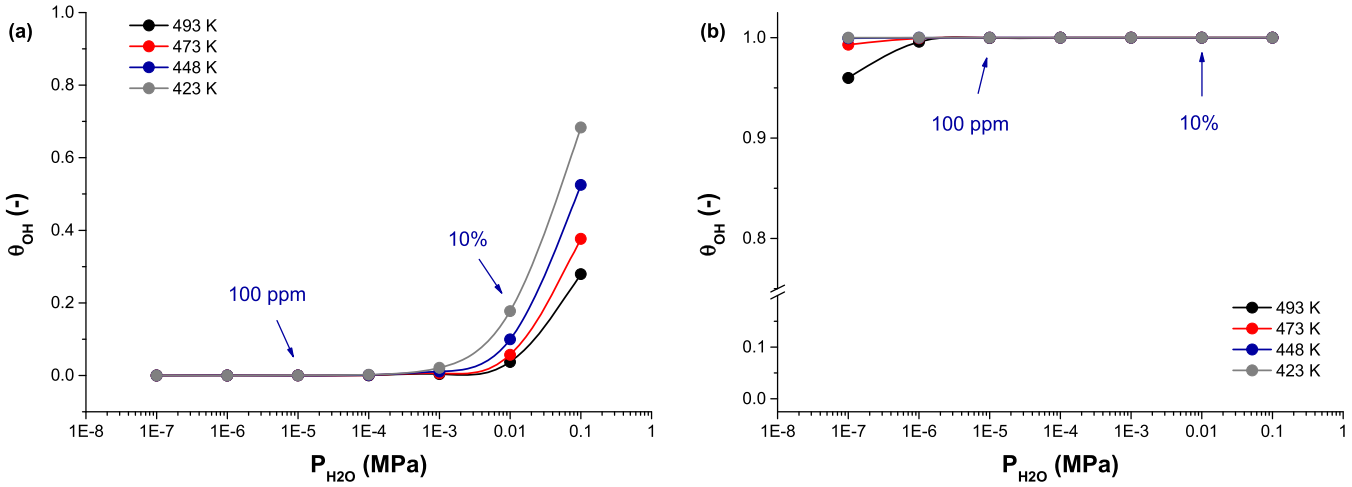

Figure 4. Thermodynamic diagrams for (a) hydrolysis alone and (b) hydrolysis + two-P formation. DFT-computed (PBE + D3) electronic energies and Gibbs free energies are provided in Supporting Information, S1.

similar reducibility in LT-RHC reactions, consistent with recent findings from us[15] and other groups.[41] Furthermore, these RHC dynamics, as extensively discussed in ref 15, can be accurately captured by a second-order transient kinetic model

$$r_{RHC} = k_{RHC} \cdot P_{NO} \cdot [Cu^{2+}]^2 \quad (3)$$

in which $ZCu^{2+}(OH)^-$ and Z_2Cu^{2+} were not differentiated but, instead, treated collectively. The success of this second-order kinetic model and the identical dynamics in Figure 2 conclude that Z_2Cu^{2+} also reacts as Cu^{2+} pairs and has similar kinetics to $ZCu^{2+}(OH)^-$ in LT-RHC. Such conclusions are reminiscent of those obtained from CO oxidation tests. Since RHC reactions generate H_2O (see R.2 and 3), the proposal of Z_2Cu^{2+} hydrolysis to $ZCu^{2+}(OH)^-$ would be valid here as well if the hydrolysis step is faster or has a similar rate as compared to LT-RHC.

Besides, R.2 and R.3 reveal that the molar ratio of H_2O generation to N_2 formation is highly dependent on the Cu^{2+} speciation, that is, $H_2O/N_2 = 2$ for $ZCu^{2+}(OH)^-$, while $H_2O/N_2 = 1$ for Z_2Cu^{2+}. Given that the experimental protocol in Figure 2 may involve both consumption of H_2O molecules via hydrolysis and generation of H_2O due to RHC reactions, we modified the protocol by starting RHC tests from steady-state SCR, where constant H_2O is produced. In this way, on one hand, we are able to decouple the two opposite effects on H_2O by stabilizing hydrolysis using steady-state SCR, and on the other hand, we can accurately measure N_2 and H_2O concentrations by avoiding feeding external percentage levels of moisture. As shown in Figure 3, constant H_2O and N_2 generation were indeed observed during steady-state SCR over aged Cu-CHA, in line with the known Standard SCR chemistry. We also calculated the turnover rates of steady-state SCR using first-order kinetics in NO and obtained 1.0×10^{-3} for 423 K, 3.1×10^{-3} for 448 K, and 8.1×10^{-3} for 473 K (unit: mol NO mol Cu^{-1} s^{-1}), consistent with literature activity results.[5,42] Note that, in this phase, a mix of Cu^{2+} and Cu^+ co-exists: subsequent cutoff of O_2 leads to RHC processes reducing all the residual Cu^{2+},[12,15] as illustrated in Figure 3 by the drop of H_2O and N_2 traces to zero and the rise of NO and NH_3 traces to their feed levels. Integrating H_2O and N_2 signals in this O_2 cutoff phase gives H_2O/N_2 ratios of 1.89 at 423 K, 1.97 at 448 K, and 2.00 at 473 K, consistent with the stoichiometry of R.2. This suggests that all the Cu^{2+} cations present in steady-state LT-SCR behave as $ZCu^{2+}(OH)^-$, even though the initial state of this aged Cu-CHA sample has a vast majority of Z_2Cu^{2+} (~80%). These data again comply with the proposal of Z_2Cu^{2+} hydrolysis to $ZCu^{2+}(OH)^-$, which likely occurs and reaches steady state during the first SCR stage of the experiments. It is also worth noticing that, contrary to CO oxidation tests, absolute dry conditions do not apply to SCR runs since H_2O is generated by the SCR reactions.

In summary, experimental results discussed so far converge to pointing out a hydrolysis reaction that converts Z_2Cu^{2+} into $ZCu^{2+}(OH)^-$. Such a scheme can reasonably explain all the observations if the hydrolysis step occurs facilely under LT-SCR conditions, that is, in the co-presence of H_2O and NH_3, and has faster or similar kinetics with respect to LT-RHC. In the following, we further challenge these premises by theoretical calculations.

3.3. First-Principles Thermodynamics and Kinetics. As accepted in the field,[5,12−14] Z_2Cu^{2+} and $ZCu^{2+}(OH)^-$ stay fully coordinated with NH_3 ligands during LT-SCR, being $Cu^{2+}(NH_3)_4$ and $Cu^{2+}(OH)^-(NH_3)_3$, respectively. In light of this, we calculated the reaction energy of the hydrolysis step (R.4) in terms of Gibbs free energies (ΔG) at standard pressure (0.1 MPa) and temperatures of interest (423−493 K). The AIMD + DFT-optimized structures are provided in Figure S1 of the Supporting Information.

$$Cu^{2+}(NH_3)_4 + H_2O \leftrightarrow Cu^{2+}(OH)^-(NH_3)_3 + NH_4^+ \quad (R.4)$$

Relating these free energies to the fraction of $Cu^{2+}(OH)^-(NH_3)_3$ at equilibrium (θ_{OH}) through the van't Hoff equation gives

$$\theta_{OH} = \frac{\exp(-\Delta G/RT) \cdot P_{H_2O}}{1 + \exp(-\Delta G/RT) \cdot P_{H_2O}} \quad (4)$$

where R is the gas constant (8.3145 J mol^{-1} K^{-1}), T is the temperature (K), and P_{H_2O} is the partial pressure of H_2O (MPa). The NH_4^+ coverage ($\sigma_{NH_4^+}$) is not included here because in continuous NH_3 flow, saturation of Brønsted acid sites by NH_4^+ is always expected, thus $\sigma_{NH_4^+} = 1$ is assumed in eq 4. Based on eq 4 and DFT-derived ΔG, we constructed a thermodynamic diagram in Figure 4a, which illustrates the

https://doi.org/10.1021/acscatal.1c02761
ACS Catal. 2021, 11, 11616−11625

variation of θ_{OH} as a function of temperatures and H_2O concentrations.

Apparently, in the considered range of temperature (423−493 K) and H_2O partial pressure (100 ppm to 10% v/v, corresponding to the levels of the RHC tests in Figure 3 and of the CO oxidation tests in Figure 1, respectively), θ_{OH} is very low, less than 20%, suggesting that the extent of hydrolysis (R.4) is rather limited. This theoretical prediction, however, contradicts our experimental observations in Figures 1−3 where almost complete hydrolysis is expected. Notice, however, that $Cu^{2+}(OH)^-(NH_3)_3$ has a thermodynamic driving force to cohabit with a counterpart in the same CHA cage to form a two-P structure (R.5), the latter species being more stable by $\Delta G = -79$ kJ mol^{-1} at 423 K.[14]

$$Cu^{2+}(OH)^-(NH_3)_3 + Cu^{2+}(OH)^-(NH_3)_3 \leftrightarrow \text{two-P} \quad \text{(R.5)}$$

Such an exergonic pairing process would thus favor the overall energetics by summing R.4 and R.5, which leads to a totally different scenario shown in Figure 4b: now, the predicted θ_{OH} is ∼100% in the range of interest, consistent with the above-reported experimental observations. Furthermore, the two-P structure has two Cu^{2+} cations and complies, therefore, with the dinuclear pathways expected for both LT-RHC and CO oxidation. Considering the exergonic nature of these two reactions, a cascade of (i) $Cu^{2+}(NH_3)_4$ hydrolysis to $Cu^{2+}(OH)^-(NH_3)_3$, (ii) pairing of $Cu^{2+}(OH)^-(NH_3)_3$ to the two-P, and (iii) two-P further scavenged by LT-RHC or CO oxidation are thermodynamically favorable and agree with all experimental results. It is also worth mentioning that the exergonic pairing process is disposable and thus is no longer available once completed. This would limit the final extent of hydrolysis when two-P scavenging reactions are absent because some $Cu^{2+}(OH)^-(NH_3)_3$ units within two-P may dehydrate back to $Cu^{2+}(NH_3)_4$ (see details in Supporting Information, S2).

Furthermore, we calculated the activation energy (E_a) of R.4 to assess the hydrolysis kinetics. As shown in Figure 5, an initial state of $Cu^{2+}(NH_3)_4$ with a proximal H_2O molecule progressively liberates one NH_3 ligand, concurrently with H_2O approaching and adsorption, and passes over a transition state of $Cu^{2+}(H_2O)(NH_3)_3$ with an adsorbed NH_3 on a nearby Brønsted acid site. Afterward, the adsorbed H_2O dissociates and one H^+ moves to the adsorbed NH_3 to form the final state of $Cu^{2+}(OH)^-(NH_3)_3 + NH_4^+$. This hydrolysis step shows a barrier of 66 kJ mol^{-1}, comparable to that of the two-P-based LT-RHC mechanism (E_a = 60 kJ mol^{-1}),[14] which thus suggests comparable reaction kinetics of the two processes. Such a theoretical prediction aligns with the RHC experiment results in Figure 2: $Cu^{2+}(NH_3)_4$ hydrolysis to $Cu^{2+}(OH)^-(NH_3)_3$ proceeds in parallel to LT-RHC over paired $Cu^{2+}(OH)^-(NH_3)_3$, so that these two processes are kinetically indistinguishable and result in identical apparent dynamics regardless of the initial $ZCu^{2+}(OH)^-$ population. Therefore, these computational results thermodynamically and kinetically rationalize the proposal of Z_2Cu^{2+} hydrolysis to $ZCu^{2+}(OH)^-$ in the presence of NH_3.

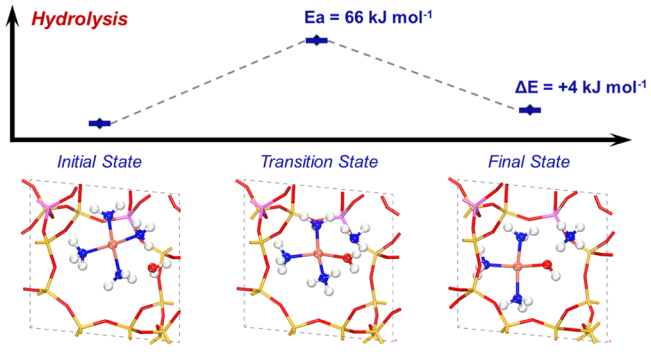

Figure 5. DFT-computed (PBE + D3) activation energy (E_a) and reaction energy (ΔE) for the hydrolysis process. Structures of the initial state, transition state, and final state are also displayed. Red: O, blue: N, white: H, yellow: Si, magenta: Al, and pink: Cu. Reaction energies calculated by PBE + D3 (+4 kJ mol^{-1}) and HSE06 + D3 (+7 kJ mol^{-1}) are very similar, rationalizing the use of PBE + D3 in this case.

Next, we turn to in situ spectroscopy to directly probe the structural variation of Cu-CHA induced by hydrolysis.

3.4. In Situ Spectroscopic Validation. Occurrence of hydrolysis, R.4, would convert Z_2Cu^{2+} into $ZCu^{2+}(OH)^-$ (NH_3-solvated form), together with the transformation of NH_3 ligands (Lewis type: L-NH_3) into NH_4^+ ions (Brønsted type: B-NH_4^+). In line with this chemistry, we expect, therefore, a decrease in Z_2Cu^{2+} and L-NH_3 and an increase in $ZCu^{2+}(OH)^-$ and B-NH_4^+. To challenge this expectation, we used in situ FTIR spectroscopy to directly characterize the structure of Cu-CHA before and after hydrolysis. Figure 6 shows the spectra of NH_3 adsorption on aged Cu-CHA at 473 K for 1 h in the absence (black) or presence (blue) of 2% H_2O. Note that 10% O_2 was kept in the feed stream to prevent possible reduction by NH_3. According to dedicated steady-state NH_3 oxidation tests by us (Table S3) and literature results by Gao et al.,[42] oxidation of NH_3 at 473 K is quite limited on Cu-CHA; thus, its occurrence is disregarded here. During the wet test, H_2O was fed 0.5 h ahead of NH_3 adsorption in order to check the hydrolysis by H_2O alone; this part of the data will be discussed in Section 3.5.

As displayed in Figure 6, negative bands at 899 and 947 cm^{-1} for T−O−T vibrations perturbed by Z_2Cu^{2+} and $ZCu^{2+}(OH)^-$, respectively, appear under both dry and wet conditions, suggesting that these two Cu^{2+} cations are coordinated with NH_3 ligands and detached from the zeolite framework.[43−45] Consistent with this, bands at 1456 cm^{-1} for B-NH_4^+, 1620 cm^{-1} for L-NH_3, and 3100−3400 cm^{-1} for stretching of adsorbed NH_3 were observed, thus confirming NH_3 adsorption on Cu^{2+} cations and Brønsted acid sites, as further supported by the consumption of bridging Si−(OH)−Al (3580 and 3608 cm^{-1}, Brønsted acid sites) and $Cu^{2+}(OH)^-$ (3653 cm^{-1}).[43−45] When comparing the dry and wet spectra, intensities of NH_3 adspecies decrease moderately in the presence of H_2O, suggesting that H_2O affects the NH_3 storage capacity on Cu-CHA. We further calculated the intensity ratio of B-NH_4^+ to L-NH_3 to qualitatively reveal their relative change; the wet B/L ratio of 2.67, as compared to 2.19 for the dry condition, indicates a greater persistence of B-NH_4^+ through H_2O exposure. Such a persistence may relate to the stronger binding strength of B-NH_4^+[5,12,14] and may also benefit from the conversion of L-NH_3 into B-NH_4^+ described by R.4. Therefore, although this observation cannot conclusively confirm the occurrence of hydrolysis, it certainly does not contradict its existence.

On the other hand, the absolute intensities of Z_2Cu^{2+} and $ZCu^{2+}(OH)^-$ show an opposite change, with an increase in $ZCu^{2+}(OH)^-$ (947 cm^{-1}) versus a decrease in Z_2Cu^{2+} (899

https://doi.org/10.1021/acscatal.1c02761
ACS Catal. 2021, 11, 11616−11625

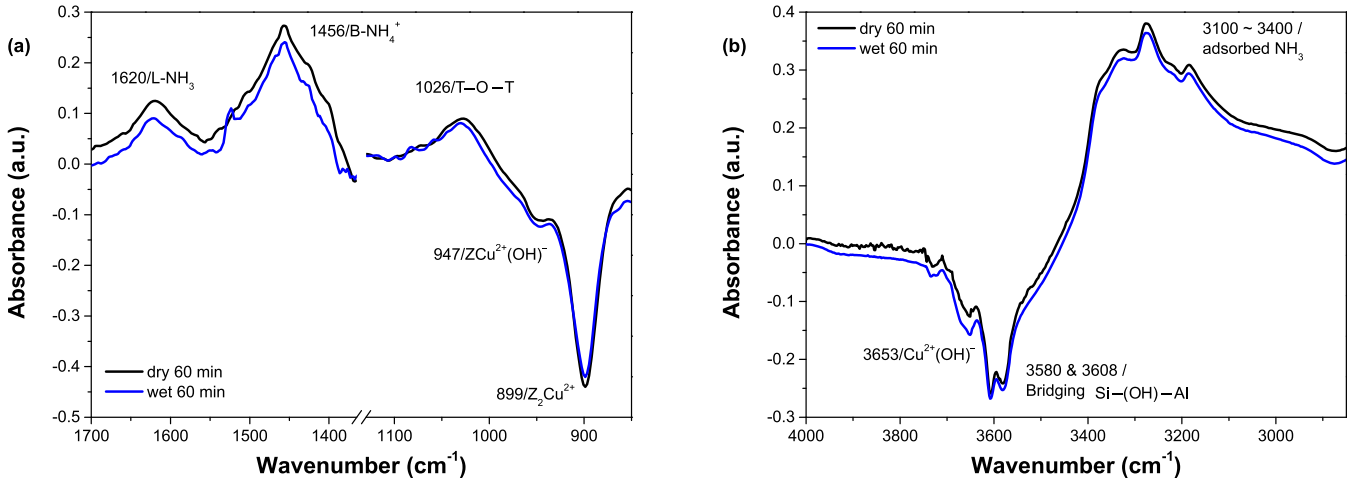

Figure 6. In situ FTIR spectra of NH_3 adsorption at 473 K for 1 h on aged Cu-CHA (Cu = 2 wt %, Si/Al = 13.5): dry (black) vs wet (blue). Reaction conditions: NH_3 = 500 ppm, O_2 = 10%, H_2O = 2% (when used), and total flow rate = 200,000 $cm^3\ h^{-1}\ g_{cat}^{-1}$ (STP). The spectra recorded during NH_3 adsorption from 30 s to 1 h are provided in Supporting Information, S2.

cm^{-1}) due to the presence of H_2O. Also, bands of bridging −OH (3580 and 3608 cm^{-1}) and $Cu^{2+}(OH)^-$ (3653 cm^{-1}) become more negative under wet conditions, as displayed in Figure 6b, indicating an increment of such sites. All these observations thus directly support the hydrolysis reaction R.4, that is, Z_2Cu^{2+} is converted into $ZCu^{2+}(OH)^-$, resulting in a newly formed Brønsted acid site. We note that the spectra changes observed here are relatively small as compared to the almost complete hydrolysis revealed by both CO oxidation and RHC experiments; this is because in the absence of two-P scavenging reactions, as for the in situ FTIR conditions here (under the steady-state flow of NH_3 + H_2O), some $Cu^{2+}(OH)^-(NH_3)_3$ units within two-P may dehydrate back to $Cu^{2+}(NH_3)_4$, which thus leads to an eventually lower hydrolysis extent (see details in Supporting Information, S2).

In conclusion, so far, hydrolysis of Z_2Cu^{2+} to $ZCu^{2+}(OH)^-$ in the presence of NH_3 has been systematically verified by multiple independent approaches including transient kinetic, in situ spectroscopic, and theoretical techniques. In the following, we try to explore whether such a hydrolysis step also proceeds in the absence of NH_3.

3.5. Hydrolysis in the Absence of NH_3. Similar to Figure 4, we constructed a DFT-based thermodynamic diagram for Z_2Cu^{2+} hydrolysis to $ZCu^{2+}(OH)^-$ in the absence of NH_3 (R.6), as shown in Figure S7.

$$Z_2Cu^{2+} + H_2O \leftrightarrow ZCu^{2+}(OH)^- + ZH^+ \quad \text{(R.6)}$$

The predicted hydrolysis extent is negligible in the whole tested range (θ_{OH} < 0.01, Figure S7), suggesting that this process is thermodynamically unfavorable (ΔG > 30 kJ mol^{-1}, Table S4). Furthermore, as reported by Luo et al.,[46] the apparent activation barrier for $ZCu^{2+}(OH)^-$ hydrothermally aging to Z_2Cu^{2+}, that is, the reverse of R.6, is as high as 168 kJ mol^{-1}. Combining this value with the current DFT-computed reaction energy of R.6 (ΔE = −23 kJ mol^{-1}) gives a high barrier of 145 kJ mol^{-1} for R.6, thus indicating a kinetically unfavorable occurrence of this step at low temperatures such as 473 K. In summary, theory predicts that hydrolysis is unfavorable when NH_3 is absent, while it becomes favorable in the presence of NH_3. A possible interpretation accounting for the NH_3 promotional effect on hydrolysis may relate to the exothermic adsorption of the detached NH_3 on Brønsted acid sites. Indeed, as displayed in Figure 5, NH_3 adsorption already takes place in the transition state, which may help stabilize it and reduce the barrier accordingly. Next, we turn to experiments to further assess the "NH_3-free" hydrolysis and challenge the predictions from theory.

We first tried to use in situ FTIR spectroscopy to directly probe the structure of Cu-CHA during H_2O exposure in the absence of NH_3. Unfortunately, signals due to molecular H_2O adsorption cover the bands of interest such as $Cu^{2+}(OH)^-$ (3653 cm^{-1}, Supporting Information, S2), thus failing to provide useful information for the analysis of the hydrolysis process. Therefore, we turned to transient CO oxidation experiments. To assess the "NH_3-free" hydrolysis, we modified the experimental protocol used in Figure 1 by just removing the NH_3 adsorption step, so that here the preoxidized Cu-CHA was directly exposed either to CO (dry) or to CO + H_2O (wet). Interestingly, in this case, H_2O did not show any significant promotion of the CO_2 formation, as shown in Figure 7, both dry and wet CO_2 formations being rather

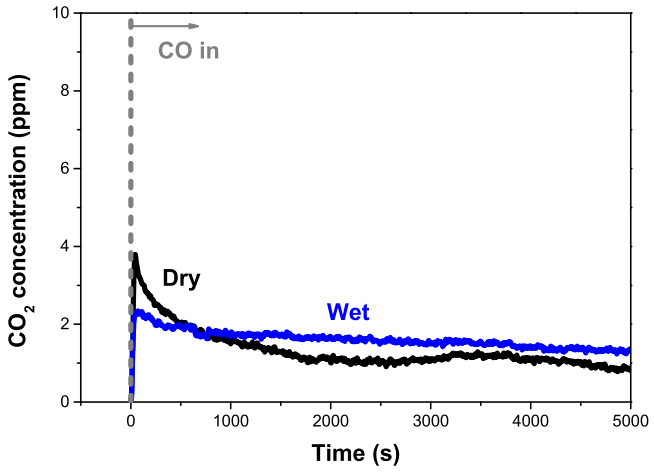

Figure 7. Transient CO oxidation tests over conditioned Cu-CHA (Cu = 1.7 wt %, Si/Al = 12.5) in the absence of NH_3: dry (black) vs wet (blue). Reaction conditions: T = 473 K, CO = 1000 ppm, O_2 = 0%, H_2O = 5% (for the wet test), and total flow rate = 266,250 $cm^3\ h^{-1}\ g_{cat}^{-1}$ (STP).

https://doi.org/10.1021/acscatal.1c02761
ACS Catal. 2021, 11, 11616−11625

limited, as compared to those in Figure 1 (with NH_3 present). These observations suggest that "NH_3-free" CO oxidation pathways, such as $CO + H_2O + 2Cu^{2+} \rightarrow CO_2 + 2Cu^{+} + 2H^{+}$, are incompatible with our present case because, on one hand, NH_3 is critical to the CO oxidation chemistry due to its mobilization of Cu^{2+} cations in favor of forming dinuclear Cu^{2+} species,[18] as discussed above, while on the other hand, H_2O is not effective in promoting CO oxidation in the absence of NH_3. The latter behavior may be due to either the inactivity of H_2O alone in hydrolyzing Z_2Cu^{2+} to $ZCu^{2+}(OH)^{-}$ or the immobilization of newly formed $ZCu^{2+}(OH)^{-}$ when NH_3 is absent. Considering the theory predictions in Figure S7, we conclude that the hydrolysis process converting Z_2Cu^{2+} into $ZCu^{2+}(OH)^{-}$ needs both H_2O and NH_3. Note that LT-SCR conditions (e.g., the LT-RHC tests in Figures 2 and 3) fully fulfill this requirement as both NH_3 and H_2O are intrinsically always present: we thus expect that NH_3-assisted hydrolysis (i.e., R.4), which is both kinetically and thermodynamically favorable, plays a role in the LT-SCR chemistry and should be therefore taken into account especially when discussing SCR reaction mechanisms over Z_2Cu^{2+}.

4. CONCLUSIONS

This work addresses the unsettled debate on how Z_2Cu^{2+} participates in LT-SCR reactions, showing identical kinetics to $ZCu^{2+}(OH)^{-}$ in both steady-state LT-SCR and transient LT-RHC. In particular, a dispute originates from the fact that the Cu reduction process involves two Cu^{2+} cations, while NH_3-solvated Z_2Cu^{2+} is only intracage mobile. Here, we provide a plausible scheme with a facile hydrolysis of Z_2Cu^{2+} to $ZCu^{2+}(OH)^{-}$, a thermodynamically and kinetically favorable process under LT-SCR conditions, which may reconcile the aforementioned open issue. Indeed, we have used transient CO oxidation as a probe reaction, together with transient RHC kinetic experiments starting from both fully oxidized and steady-state SCR conditions, in situ FTIR spectroscopy, and first-principles calculations of DFT and AIMD, to collect evidence from multiple perspectives, including in situ quantifications of available $ZCu^{2+}(OH)^{-}$, reaction kinetics and stoichiometry of $ZCu^{2+}(OH)^{-}/Z_2Cu^{2+}$ involved in LT-RHC, direct structural characterization of Cu-CHA induced by hydrolysis, and detailed thermodynamics and kinetics of the hydrolysis step. Such an integrated, multitechnique approach reveals unambiguously that the hydrolysis of Z_2Cu^{2+} to $ZCu^{2+}(OH)^{-}$ does proceed in the presence of NH_3, while it does not occur in the NH_3-free case. Accordingly, we infer that the NH_3-assisted hydrolysis process plays a critical role in the LT-SCR chemistry and should be considered especially when discussing reaction mechanisms over Z_2Cu^{2+}.

While the conclusions above apply to the Cu-CHA catalysts herein investigated, effects of Cu-CHA composition (e.g., Si/Al ratio, Cu loading) and of hydrothermal treatments on the hydrolysis process remain to be assessed. Likewise, the competition between hydrolysis and other reaction steps, as well as its relevance in the overall LT-SCR reaction network, still requires further clarification. These aspects will be tackled in forthcoming follow-up studies.

■ ASSOCIATED CONTENT

Supporting Information

The Supporting Information is available free of charge at https://pubs.acs.org/doi/10.1021/acscatal.1c02761.

Additional computational results, in situ FTIR spectroscopy images, and kinetic results and discussion (PDF)

■ AUTHOR INFORMATION

Corresponding Authors

Xiang Gao − *State Key Laboratory of Clean Energy Utilization, State Environmental Protection Center for Coal-Fired Air Pollution Control, Zhejiang University, Hangzhou 310027, China;* orcid.org/0000-0002-1732-2132; Phone: +86 571 87951335; Email: xgao1@zju.edu.cn

Enrico Tronconi − *Laboratory of Catalysis and Catalytic Processes, Dipartimento di Energia, Politecnico di Milano, Milano 20156, Italy;* orcid.org/0000-0002-5472-2696; Phone: +39 02 23993264; Email: enrico.tronconi@polimi.it

Authors

Wenshuo Hu − *State Key Laboratory of Clean Energy Utilization, State Environmental Protection Center for Coal-Fired Air Pollution Control, Zhejiang University, Hangzhou 310027, China;* orcid.org/0000-0001-8280-1167

Umberto Iacobone − *Laboratory of Catalysis and Catalytic Processes, Dipartimento di Energia, Politecnico di Milano, Milano 20156, Italy*

Federica Gramigni − *Laboratory of Catalysis and Catalytic Processes, Dipartimento di Energia, Politecnico di Milano, Milano 20156, Italy*

Yu Zhang − *State Key Laboratory of Clean Energy Utilization, State Environmental Protection Center for Coal-Fired Air Pollution Control, Zhejiang University, Hangzhou 310027, China*

Xiaoxiang Wang − *Institute of Industrial Ecology and Environment, College of Chemical and Biological Engineering, Zhejiang University, Hangzhou 310027, China*

Shaojun Liu − *State Key Laboratory of Clean Energy Utilization, State Environmental Protection Center for Coal-Fired Air Pollution Control, Zhejiang University, Hangzhou 310027, China;* orcid.org/0000-0003-0976-5707

Chenghang Zheng − *State Key Laboratory of Clean Energy Utilization, State Environmental Protection Center for Coal-Fired Air Pollution Control, Zhejiang University, Hangzhou 310027, China*

Isabella Nova − *Laboratory of Catalysis and Catalytic Processes, Dipartimento di Energia, Politecnico di Milano, Milano 20156, Italy;* orcid.org/0000-0001-7239-2785

Complete contact information is available at: https://pubs.acs.org/10.1021/acscatal.1c02761

Notes

The authors declare no competing financial interest.

■ ACKNOWLEDGMENTS

Authors from Zhejiang University acknowledge the financial support from the National Natural Science Foundation of China (51836006 and 52006192) and Development Plan of Shandong Province of China (2020CXGC011401) and also thank Shanghai Supercomputer Center for the computing time.

■ REFERENCES

(1) Beale, A. M.; Gao, F.; Lezcano-Gonzalez, I.; Peden, C. H. F.; Szanyi, J. Recent advances in automotive catalysis for NOx emission

control by small-pore microporous materials. *Chem. Soc. Rev.* **2015**, *44*, 7371−7405.
(2) Borfecchia, E.; Beato, P.; Svelle, S.; Olsbye, U.; Lamberti, C.; Bordiga, S. Cu-CHA - a model system for applied selective redox catalysis. *Chem. Soc. Rev.* **2018**, *47*, 8097−8133.
(3) Gao, F.; Szanyi, J. On the hydrothermal stability of Cu/SSZ-13 SCR catalysts. *Appl. Catal., A* **2018**, *560*, 185−194.
(4) Lomachenko, K. A.; Borfecchia, E.; Negri, C.; Berlier, G.; Lamberti, C.; Beato, P.; Falsig, H.; Bordiga, S. The Cu-CHA deNOx Catalyst in Action: Temperature-Dependent NH_3-Assisted Selective Catalytic Reduction Monitored by Operando XAS and XES. *J. Am. Chem. Soc.* **2016**, *138*, 12025−12028.
(5) Paolucci, C.; Parekh, A. A.; Khurana, I.; Di Iorio, J. R.; Li, H.; Albarracin Caballero, J. D.; Shih, A. J.; Anggara, T.; Delgass, W. N.; Miller, J. T.; Ribeiro, F. H.; Gounder, R.; Schneider, W. F. Catalysis in a Cage: Condition-Dependent Speciation and Dynamics of Exchanged Cu Cations in SSZ-13 Zeolites. *J. Am. Chem. Soc.* **2016**, *138*, 6028−6048.
(6) Marberger, A.; Petrov, A. W.; Steiger, P.; Elsener, M.; Kröcher, O.; Nachtegaal, M.; Ferri, D. Time-resolved copper speciation during selective catalytic reduction of NO on Cu-SSZ-13. *Nat. Catal.* **2018**, *1*, 221−227.
(7) Wang, A.; Chen, Y.; Walter, E. D.; Washton, N. M.; Mei, D.; Varga, T.; Wang, Y.; Szanyi, J.; Wang, Y.; Peden, C. H. F.; Gao, F. Unraveling the mysterious failure of Cu/SAPO-34 selective catalytic reduction catalysts. *Nat. Commun.* **2019**, *10*, 1137.
(8) Paolucci, C.; Verma, A. A.; Bates, S. A.; Kispersky, V. F.; Miller, J. T.; Gounder, R.; Delgass, W. N.; Ribeiro, F. H.; Schneider, W. F. Isolation of the copper redox steps in the standard selective catalytic reduction on Cu-SSZ-13. *Angew. Chem., Int. Ed.* **2014**, *53*, 11828−11833.
(9) Janssens, T. V. W.; Falsig, H.; Lundegaard, L. F.; Vennestrøm, P. N. R.; Rasmussen, S. B.; Moses, P. G.; Giordanino, F.; Borfecchia, E.; Lomachenko, K. A.; Lamberti, C.; Bordiga, S.; Godiksen, A.; Mossin, S.; Beato, P. A Consistent Reaction Scheme for the Selective Catalytic Reduction of Nitrogen Oxides with Ammonia. *ACS Catal.* **2015**, *5*, 2832−2845.
(10) Gao, F.; Mei, D.; Wang, Y.; Szanyi, J.; Peden, C. H. F. Selective Catalytic Reduction over Cu/SSZ-13: Linking Homo- and Heterogeneous Catalysis. *J. Am. Chem. Soc.* **2017**, *139*, 4935−4942.
(11) Partridge, W. P.; Joshi, S. Y.; Pihl, J. A.; Currier, N. W. New operando method for quantifying the relative half-cycle rates of the NO SCR redox cycle over Cu-exchanged zeolites. *Appl. Catal., B* **2018**, *236*, 195−204.
(12) Villamaina, R.; Liu, S.; Nova, I.; Tronconi, E.; Ruggeri, M. P.; Collier, J.; York, A.; Thompsett, D. Speciation of Cu Cations in Cu-CHA Catalysts for NH_3-SCR: Effects of SiO_2/AlO_3 Ratio and Cu-Loading Investigated by Transient Response Methods. *ACS Catal.* **2019**, *9*, 8916−8927.
(13) Liu, C.; Kubota, H.; Amada, T.; Kon, K.; Toyao, T.; Maeno, Z.; Ueda, K.; Ohyama, J.; Satsuma, A.; Tanigawa, T.; Tsunoji, N.; Sano, T.; Shimizu, K. i. In Situ Spectroscopic Studies on the Redox Cycle of NH_3−SCR over Cu−CHA Zeolites. *ChemCatChem* **2020**, *12*, 3050−3059.
(14) Hu, W.; Selleri, T.; Gramigni, F.; Fenes, E.; Rout, K. R.; Liu, S.; Nova, I.; Chen, D.; Gao, X.; Tronconi, E. On the Redox Mechanism of Low-Temperature NH_3-SCR over Cu-CHA: A Combined Experimental and Theoretical Study of the Reduction Half Cycle. *Angew. Chem., Int. Ed.* **2021**, *60*, 7197−7204.
(15) Gramigni, F.; Nasello, N. D.; Usberti, N.; Iacobone, U.; Selleri, T.; Hu, W.; Liu, S.; Gao, X.; Nova, I.; Tronconi, E. Transient Kinetic Analysis of Low-Temperature NH_3-SCR over Cu-CHA Catalysts Reveals a Quadratic Dependence of Cu Reduction Rates on Cu^{II}. *ACS Catal.* **2021**, *11*, 4821−4831.
(16) Usberti, N.; Gramigni, F.; Nasello, N. D.; Iacobone, U.; Selleri, T.; Hu, W.; Liu, S.; Gao, X.; Nova, I.; Tronconi, E. An experimental and modelling study of the reactivity of adsorbed NH_3 in the low temperature NH_3-SCR reduction half-cycle over a Cu-CHA catalyst. *Appl. Catal., B* **2020**, *279*, 119397.
(17) Paolucci, C.; Khurana, I.; Parekh, A. A.; Li, S.; Shih, A. J.; Li, H.; Di Iorio, J. R.; Albarracin-Caballero, J. D.; Yezerets, A.; Miller, J. T.; Delgass, W. N.; Ribeiro, F. H.; Schneider, W. F.; Gounder, R. Dynamic multinuclear sites formed by mobilized copper ions in NOx selective catalytic reduction. *Science* **2017**, *357*, 898−903.
(18) Villamaina, R.; Iacobone, U.; Nova, I.; Ruggeri, M. P.; Collier, J.; Thompsett, D.; Tronconi, E. Low-T CO Oxidation over Cu−CHA Catalysts in Presence of NH_3: Probing the Mobility of Cu^{II} Ions and the Role of Multinuclear Cu^{II} Species. *ChemCatChem* **2020**, *12*, 3843−3848.
(19) Paolucci, C.; Di Iorio, J. R.; Schneider, W. F.; Gounder, R. Solvation and Mobilization of Copper Active Sites in Zeolites by Ammonia: Consequences for the Catalytic Reduction of Nitrogen Oxides. *Acc. Chem. Res.* **2020**, *53*, 1881−1892.
(20) Da Costa, P.; Modén, B.; Meitzner, G. D.; Lee, D. K.; Iglesia, E. Spectroscopic and chemical characterization of active and inactive Cu species in NO decomposition catalysts based on Cu-ZSM5. *Phys. Chem. Chem. Phys.* **2002**, *4*, 4590−4601.
(21) Daya, R.; Joshi, S. Y.; Luo, J.; Dadi, R. K.; Currier, N. W.; Yezerets, A. On kinetic modeling of change in active sites upon hydrothermal aging of Cu-SSZ-13. *Appl. Catal., B* **2020**, *263*, 118368.
(22) Daya, R.; Trandal, D.; Dadi, R. K.; Li, H.; Joshi, S. Y.; Luo, J.; Kumar, A.; Yezerets, A. Kinetics and thermodynamics of ammonia solvation on Z_2Cu, ZCuOH and ZCu sites in Cu-SSZ-13 − Implications for hydrothermal aging. *Appl. Catal., B* **2021**, *297*, 120444.
(23) Hu, W.; Zhang, Y.; Liu, S.; Zheng, C.; Gao, X.; Nova, I.; Tronconi, E. Improvement in activity and alkali resistance of a novel V-$Ce(SO_4)_2$/Ti catalyst for selective catalytic reduction of NO with NH_3. *Appl. Catal., B* **2017**, *206*, 449−460.
(24) Hu, W.; Zhang, S.; Xin, Q.; Zou, R.; Zheng, C.; Gao, X.; Cen, K. Mechanistic investigation of NH_3 oxidation over V-0.5$Ce(SO_4)_2$/Ti NH_3-SCR catalyst. *Catal. Commun.* **2018**, *112*, 1−4.
(25) Maestri, M.; Iglesia, E. First-principles theoretical assessment of catalysis by confinement: NO-O_2 reactions within voids of molecular dimensions in siliceous crystalline frameworks. *Phys. Chem. Chem. Phys.* **2018**, *20*, 15725−15735.
(26) Chen, L.; Falsig, H.; Janssens, T. V. W.; Grönbeck, H. Activation of oxygen on $(NH_3\text{-}Cu\text{-}NH_3)^+$ in NH_3-SCR over Cu-CHA. *J. Catal.* **2018**, *358*, 179−186.
(27) Chen, L.; Janssens, T. V. W.; Vennestrøm, P. N. R.; Jansson, J.; Skoglundh, M.; Grönbeck, H. A Complete Multisite Reaction Mechanism for Low-Temperature NH_3-SCR over Cu-CHA. *ACS Catal.* **2020**, *10*, 5646−5656.
(28) Perdew, J. P.; Burke, K.; Ernzerhof, M. Generalized gradient approximation made simple. *Phys. Rev. Lett.* **1996**, *77*, 3865−3868.
(29) Grimme, S.; Antony, J.; Ehrlich, S.; Krieg, H. A consistent and accurate ab initio parametrization of density functional dispersion correction (DFT-D) for the 94 elements H-Pu. *J. Chem. Phys.* **2010**, *132*, 154104.
(30) Grimme, S.; Ehrlich, S.; Goerigk, L. Effect of the damping function in dispersion corrected density functional theory. *J. Comput. Chem.* **2011**, *32*, 1456−1465.
(31) Nosé, S. A unified formulation of the constant temperature molecular dynamics methods. *J. Chem. Phys.* **1984**, *81*, 511−519.
(32) Hoover, W. G. Canonical dynamics: Equilibrium phase-space distributions. *Phys. Rev. A: At., Mol., Opt. Phys.* **1985**, *31*, 1695−1697.
(33) Kresse, G.; Furthmüller, J. Efficient iterative schemes forab initiototal-energy calculations using a plane-wave basis set. *Phys. Rev. B: Condens. Matter Mater. Phys.* **1996**, *54*, 11169−11186.
(34) Blöchl, P. E. Projector augmented-wave method. *Phys. Rev. B: Condens. Matter Mater. Phys.* **1994**, *50*, 17953−17979.
(35) Kresse, G.; Joubert, D. From ultrasoft pseudopotentials to the projector augmented-wave method. *Phys. Rev. B: Condens. Matter Mater. Phys.* **1999**, *59*, 1758−1775.
(36) Henkelman, G.; Uberuaga, B. P.; Jónsson, H. A climbing image nudged elastic band method for finding saddle points and minimum energy paths. *J. Chem. Phys.* **2000**, *113*, 9901−9904.

(37) Heyd, J.; Scuseria, G. E.; Ernzerhof, M. Hybrid functionals based on a screened Coulomb potential. *J. Chem. Phys.* **2003**, *118*, 8207−8215.
(38) Heyd, J.; Scuseria, G. E. Efficient hybrid density functional calculations in solids: assessment of the Heyd-Scuseria-Ernzerhof screened Coulomb hybrid functional. *J. Chem. Phys.* **2004**, *121*, 1187−1192.
(39) Heyd, J.; Scuseria, G. E.; Ernzerhof, M. Hybrid functionals based on a screened Coulomb potential. *J. Chem. Phys.* **2003**, *118*, 8207.
(40) Campbell, C. T.; Sellers, J. R. V. The entropies of adsorbed molecules. *J. Am. Chem. Soc.* **2012**, *134*, 18109−18115.
(41) Ma, Y.; Wu, X.; Ding, J.; Liu, L.; Jin, B.; Walter, E. D.; Ran, R.; Si, Z.; Gao, F.; Weng, D. Quasi-operando quantification of Cu^{II} ions in Cu-SSZ-13 catalyst by an NH_3 temperature-programmed reduction method. *Chem. Commun.* **2021**, *57*, 1891−1894.
(42) Gao, F.; Walter, E. D.; Kollar, M.; Wang, Y.; Szanyi, J.; Peden, C. H. F. Understanding ammonia selective catalytic reduction kinetics over Cu/SSZ-13 from motion of the Cu ions. *J. Catal.* **2014**, *319*, 1−14.
(43) Luo, J.; Gao, F.; Kamasamudram, K.; Currier, N.; Peden, C. H. F.; Yezerets, A. New insights into Cu/SSZ-13 SCR catalyst acidity. Part I: Nature of acidic sites probed by NH_3 titration. *J. Catal.* **2017**, *348*, 291−299.
(44) Lezcano-Gonzalez, I.; Deka, U.; Arstad, B.; Van Yperen-De Deyne, A.; Hemelsoet, K.; Waroquier, M.; Van Speybroeck, V.; Weckhuysen, B. M.; Beale, A. M. Determining the storage, availability and reactivity of NH_3 within Cu-Chabazite-based Ammonia Selective Catalytic Reduction systems. *Phys. Chem. Chem. Phys.* **2014**, *16*, 1639−1650.
(45) Zhang, Y.; Peng, Y.; Li, K.; Liu, S.; Chen, J.; Li, J.; Gao, F.; Peden, C. H. F. Using Transient FTIR Spectroscopy to Probe Active Sites and Reaction Intermediates for Selective Catalytic Reduction of NO on Cu/SSZ-13 Catalysts. *ACS Catal.* **2019**, *9*, 6137−6145.
(46) Luo, J.; Kamasamudram, K.; Currier, N.; Yezerets, A. NH_3-TPD methodology for quantifying hydrothermal aging of Cu/SSZ-13 SCR catalysts. *Chem. Eng. Sci.* **2018**, *190*, 60−67.

https://doi.org/10.1021/acscatal.1c02761
ACS Catal. 2021, 11, 11616−11625